JOURNAL OF SOLID STATE CHEMISTRY 13, 258–271 (1975)

First Order Magnetic Transition, Magnetic Structure, and Vacancy Distribution in Fe_2P

R. WÄPPLING, L. HÄGGSTRÖM, T. ERICSSON, S. DEVANARAYANAN,* AND E. KARLSSON

Institute of Physics, Uppsala University, Box 530, S-751 21 Uppsala 1, Sweden

AND

B. CARLSSON AND S. RUNDQVIST

Institute of Chemistry, Uppsala University, Box 531, S-751 21 Uppsala 1, Sweden

Received February 22, 1974

The para- to ferromagnetic transition in Fe_2P has been studied using Mössbauer spectroscopy. The magnetic hyperfine fields drop abruptly from about half of their saturation values to zero at 214.5 K indicating a first order transition. The isomer shifts show a discontinuous change at the transition point. For some samples the transition takes place over a wide temperature range, probably due to impurities and other imperfections in the samples. From the magnetic hyperfine fields at 15 K the magnetic moments can be deduced to be 1.14 μ_B and 1.78 μ_B for Fe(1) and Fe(2), respectively. An assignment of the components in the Mössbauer spectra to the two crystallographically nonequivalent iron positions has been made from the temperature variation of the spectra.

The ordering of metal vacancies has been investigated by a Mössbauer study of a nonstoichiometric Fe_2P sample and by an X-ray diffraction study of a nonstoichiometric Mn_2P crystal.

1. Introduction

1.1. Previous Work

The chemical and physical properties of Fe_2P have been studied in several investigations. There are, however, appreciable differences between the results reported by different investigators, particularly as regards the magnetic properties. While the actual occurrence of a paramagnetic/ferromagnetic transition in Fe_2P is well established, there is considerable disagreement between the various determinations of the Curie temperature and the saturation magnetic moment for the ferromagnetic phase (*1–9*). It appears that these discrepancies might, at least to some extent, depend on the lack of rigorous chemical and physical definition of the test samples. Small amounts of impurities and deviations from stoichiometry might affect the measurements seriously (*8*).

In a recent study (*10*) the problems in preparing high-purity Fe_2P in stoichiometric or nonstoichiometric form were critically examined. The homogeneity range of the Fe_2P phase was carefully determined for temperatures up to 1100°C. In addition, the crystal structure of pure, stoichiometric Fe_2P was accurately refined from room temperature X-ray diffraction data.

With these new results at hand we decided to reexamine Fe_2P by Mössbauer spectroscopic methods. A number of Mössbauer studies of Fe_2P have been reported previously (*5, 6, 9, 11–14*), but only limited conclusions have been drawn from the experimental information.

* Present address: Physics Department, University of Kerala, Trivandrum, India.

In the present study, our interest has been focused on three particular problems. First, we have reexamined our previously proposed assignment (*14*) of the components in the Mössbauer spectra to the two nonequivalent types of iron atom in the Fe_2P structure. Second, we have attempted to determine the type of defects occurring in the structure of nonstoichiometric Fe_2P. In this connection we found it interesting to compare the situation in Fe_2P with that in the isostructural compound Mn_2P (*15*). We have therefore included an X-ray diffraction study of a nonstoichiometric Mn_2P crystal. Third, we have studied the magnetic structure of Fe_2P and the behavior at temperatures in the vicinity of the magnetic transition in order to examine the unusual temperature dependence of the Mössbauer spectrum as mentioned by Roger (*6*).

1.2. The Crystal Structure of Fe_2P

For the purposes of the following discussions a brief description of the crystal structure of Fe_2P is given here.

Accurate crystallographic data for the Fe_2P structure arch presented in (*10*), and the interatomic distances as given in Table I are reproduced from that work.

The hexagonal unit cell of Fe_2P contains six iron atoms situated on two threefold positions: Fe(1) and Fe(2), and three phosphorus atoms situated on one twofold:

TABLE I

INTERATOMIC DISTANCES IN Fe_2P (Å) (DISTANCES SHORTER THAN 3.7 Å ARE LISTED)

Fe(1)–2P(1)	2.2147(4)	Fe(2)–1P(2)	2.3787(7)
–2P(2)	2.2936(5)	–4P(1)	2.4833(2)
–2Fe(1)	2.6102(12)	–2Fe(1)	2.6301(7)
–2Fe(2)	2.6301(7)	–4Fe(1)	2.7082(4)
–4Fe(2)	2.7082(4)	–4Fe(2)	3.0873(4)
–2Fe(1)	3.4581(2)	–2Fe(2)	3.4581(2)
		–1P(2)	3.4889(7)
P(1)–3Fe(1)	2.2147(4)	P(2)–6Fe(1)	2.2936(5)
–6Fe(2)	2.4833(2)	–3Fe(2)	2.3787(7)
–3P(1)	3.3877(1)	–2P(2)	3.4581(2)
–2P(1)	3.4581(2)	–3Fe(2)	3.4889(7)

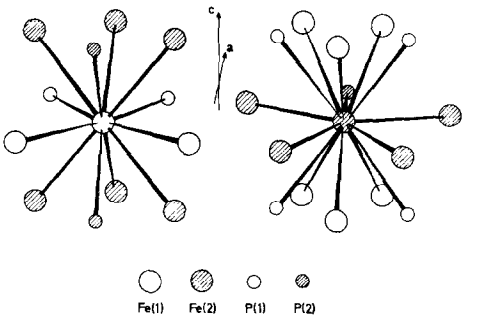

FIG. 1. The near atomic environments of Fe(1) and Fe(2) in Fe_2P.

P(1), and one singlefold: P(2), position. The crystal structure can be described in terms of coordination polyhedra of iron atoms enclosing central phosphorus atoms (*16*). An alternative description, due to Fruchart et al. (*5*), emphasizes the environment of the phosphorus atoms about the iron atoms. The Fe(1) atoms have four near phosphorus neighbors situated at the corners of a distorted tetrahedron, and the Fe(2) atoms have five phosphorus neighbors at the corners of a distorted square-based pyramid. In addition, the Fe(1) atoms have eight near iron neighbors and the Fe(2) atoms ten near iron neighbors. The near atomic environment of the two types of iron atom is illustrated in Fig. 1.

2. Experimental Details

2.1. Mössbauer Spectroscopy

For the Mössbauer spectroscopic measurements we used four different Fe_2P samples. Samples A and B were selected from the material synthesized by Carlsson et al. Detailed information on the synthetic techniques and chemical analytical results is given in (*10*). Sample A, which is identical with alloy No. 2 in (*10*), represented the closest approach to pure stoichiometric Fe_2P attained in the work by Carlsson et al., its composition being $Fe_{1.998}P$. Sample B was a nonstoichiometric Fe_2P specimen. Strongly exposed powder photographs for this material revealed no diffraction lines from phases other than Fe_2P. The lattice parameters: $a = 5.8585(3)$ Å; $c = 3.4527(3)$ Å; (throughout the text, numbers in parenthesis after numerical

values are estimated standard deviations referring to the last significant digit) indicate a composition corresponding to the formula $Fe_{1.957}P$. Sample C was taken from a large Fe_2P single crystal grown from an Fe–P melt by the Bridgman method. The starting materials for the single crystal synthesis were inferior in quality as compared with those used in the studies by Carlsson et al. (*10*), and the total impurity content of the crystal was about 0.25 weight%. A lattice parameter determination indicated a composition of $Fe_{1.99}P$ for the Fe_2P phase.

Sample D was kindly provided by Dr. D. Bellavance. It consisted of single crystals prepared by molten salt electrolysis in exactly the same manner as described by Bellavance et al. (*7*). According to this reference, the crystals should be nonstoichiometric with a composition corresponding to the formula $Fe_{1.9}P$. However, the material was later reported to contain appreciable amounts of impurities, mainly carbon contamination introduced from the graphite electrode and crucible during electrolysis (*8*). We determined the Fe_2P lattice parameters for the electrolytic crystals by the technique described in (*10*). The values deviated insignificantly from those reported in (*10*) for stoichiometric Fe_2P. A wet-chemical analysis using the methods described in (*10*) gave 77.53 wt.% iron and 21.90 wt.% phosphorus.

The samples were crushed to a fine powder, thoroughly mixed with boron nitride powder in the approximate proportions 1:15, and pressed to circular discs with 5 or 10 mg/cm^2 of natural iron. The available amount of Sample B was so small that the average surface density for this absorber was only 2 mg/cm^2.

The discs were mounted in a variable temperature cryostat or a furnace, and transmission Mössbauer spectra were recorded at typically ten different temperatures in the range 15–900 K, using a room temperature ^{57}Co*Pd* source. The temperatures were controlled to within ±0.3 degrees.

In the analysis of the Mössbauer spectra the experimental data were fitted to various sets of lorentzian lines by the least-squares method, using a modified version of the program described in (*17*) and an IBM 370/155 computer.

2.2. X-Ray Diffraction

Our X-ray crystallographic work was based on diffraction data for a nonstoichiometric Mn_2P crystal collected more than ten years ago in connection with studies of manganese phosphides (*15*). Owing to the lack of adequate computing facilities no crystal structure refinement was carried out at that time.

The crystal was picked from a two-phase Mn_2P + MnP alloy, which had been annealed at 1070°C and quenched. The lattice parameters of the Mn_2P phase as obtained by X-ray powder diffraction methods were $a = 6.059$ Å; $c = 3.440$ Å; with an estimated relative error less than 0.04%. For stoichiometric Mn_2P the cell dimensions obtained were $a = 6.081$ Å; $c = 3.460$ Å. The relationship between the composition and the lattice parameters for the Mn_2P phase has not been determined quantitatively. By comparing the results for Mn_2P (*15*) with those for Fe_2P (*10*) and assuming a similar lattice parameter versus composition relationship in the two cases, we estimated the composition of the Mn_2P phase in the quenched alloy to lie in the vicinity of 34.5 at.% phosphorus. If the single crystal selected was a representative specimen for the Mn_2P phase in the quenched alloy, its composition would thus correspond to the formula $Mn_{1.9}P$.

The crystal was mounted along the hexagonal c axis and diffraction data for the ($hk0$) reflexions were recorded in a Weissenberg camera with zirconium-filtered MoK radiation using the multiple film technique with thin iron foils as absorbers between successive films. The intensities were estimated visually by comparison with an intensity scale prepared from timed exposures of one reflexion from the crystal. The crystal had a fairly uniform cross-section of less than 0.05 mm. The effects of absorption were estimated to be very small and were neglected in the refinement. The numerical treatment of the data was carried out on an IBM 370/155 computer using standard types of crystallographic programs. In the structure

refinement 58 observed ($hk0$) reflexions were used, and weights for the observed structure factors were assigned according to Cruickshank's formula (*18*). The structure data for stoichiometric Mn_2P (*15*) served as the starting point in the refinement, which was performed by means of the full-matrix least-squares program UPALS (*19*). Atomic scattering factors and dispersion corrections were taken from (*20*) and (*21*), respectively. The following parameters were refined: one scale factor, one positional parameter for each of the two nonequivalent manganese positions, one isotropic temperature factor for each of the two manganese and the two phosphorus positions, and one occupation parameter for the Mn (1) position (keeping the occupation parameters for the remaining atoms fixed). The refinement converged rapidly. The observed structure factor values for the very strongest reflexions were, however, appreciably smaller than the calculated values, presumably due to extinction effects. A subsequent refinement, with the four strongest reflexions excluded, gave parameter values, which did not differ by more than one standard deviation from those in the first refinement. The conventional R value

$$\left(R = \frac{\sum (|F_o| - |F_c|)}{\sum |F_o|}\right)$$

with all reflexions included was 0.070, and with the four strongest reflexions excluded it was 0.061.

3. Results

3.1. Assignment of the Components in the Mössbauer Spectrum of Stoichiometric Fe_2P

The room-temperature Mössbauer spectrum of Fe_2P can be resolved into four absorption lines, two of which have a lower intensity than the remaining pair. Since there are two crystallographically nonequivalent iron atoms, Fe(1) and Fe(2), in the Fe_2P structure it seems reasonable to associate one pair of lines in the Mössbauer spectrum with each of the two types of iron atom. In a previous study (*14*) we tentatively proposed an assignment based on the following arguments. Crystal structure refinements of Mn_2P and Ni_2P, which are isostructural with Fe_2P, indicate that the thermal vibrations are larger for the Mn(2) or Ni(2) positions than for the Mn(1) or Ni(1) positions (*15*). We inferred by analogy that a similar situation prevails in Fe_2P. This implies that the recoil-free fraction for the Fe(2) atoms should be smaller than that for the Fe(1) atoms. Accordingly, we assigned the low-intensity pair of absorption lines to the Fe(2) atoms.

With the presently available information we can now reexamine the arguments on a more quantitative basis. An accurate structure refinement of a strictly stoichiometric Fe_2P crystal (*10*) has shown that there is indeed a significant difference between the thermal vibrations for Fe(1) and Fe(2). The isotropic thermal vibration parameters obtained were $B = 0.42(2)$ Å^2 for Fe(1) and $B = 0.58(2)$ Å^2 for Fe(2). The corresponding room temperature recoil-free fractions f, as calculated from the expression

$$f = e^{-(B/2\lambda^2)},$$

where λ is the gamma ray wavelength, are 0.75(1) and 0.68(1), respectively.

The analysis of the intensities in Mössbauer spectra, particularly in cases where the lines are overlapping, is complicated by the saturation effects occurring in absorbers of finite thickness. There are several ways of estimating the intensities corresponding to the ideal case of zero thickness of the absorber. One way is to measure the intensities for several absorber thicknesses and extrapolate to zero thickness.

It turns out that in order to make reasonably thin homogeneous absorbers the grain size should, due to the high recoil-free fractions in Fe_2P, be less than 1 μm. Such absorbers were prepared, but they showed very broad absorption lines probably due to strains and deformations introduced during the grinding, and they could not be used for reliable intensity measurements.

An alternative way is then to try to correct the spectra (recorded with slightly larger grains $\sim$10 μm), using theoretical expressions for the transmission of the gamma radiation through the absorbers. We used the fast Fourier transform technique (*22*) to reduce the

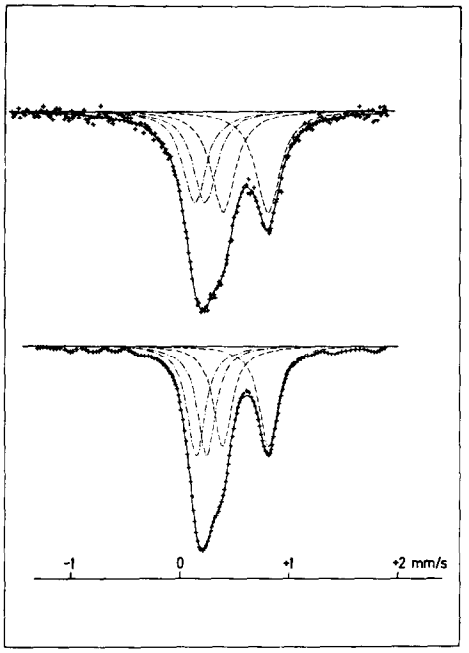

FIG. 2. Mössbauer spectrum of Fe_2P (Sample A) recorded at 295 K, and the deconvoluted absorption probability of the same spectrum (below) using the Fast Fourier Transformation (FFT). Fe(2), ----; Fe(1), -·-·-·.

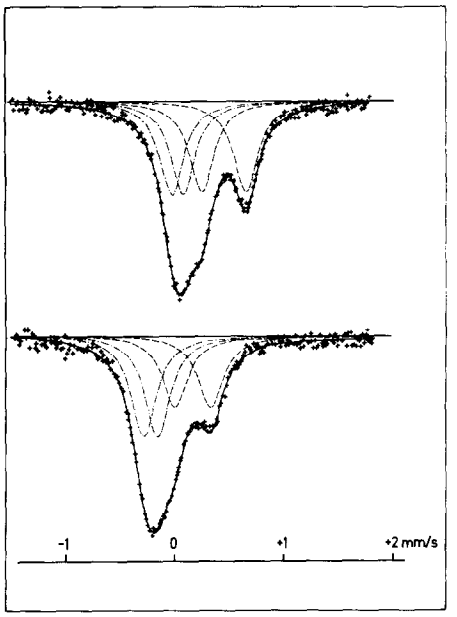

FIG. 3. Mössbauer spectra of Fe_2P (Sample A) recorded at 490 K (top) and 900 K (bottom).

room temperature spectra to the corresponding absorption probabilities in the absorber. The result depends sensitively on the local thickness of the absorber (most Mössbauer powder absorbers contain appreciable amounts of "holes") and to a lesser extent on the filtering functions and source linewidth. Figure 2 shows one measured spectrum and the corresponding absorption probability obtained using the nonresonant background estimated from the recoil-free fractions given above and an average grain size as found in a microscopic investigation of the powdered samples used. The relative intensities of the two pairs of lines in the Mössbauer spectrum change from 0.90(2):1 to 1.06(2):1. (It is to be observed that in the fitting procedure the intensity is constrained to be the same for the two lines in each pair.) The change in relative intensities is in the expected direction since the doublet buried in the central absorption maximum is most affected by the saturation effects. It is, however, still difficult to make an unambiguous assignment of the components to the crystallographic positions.

A third way to attack the problem is to study the temperature variation of the intensities in the Mössbauer spectra, as exemplified in Fig. 3. From the room temperature f-factors given above, the Debye temperatures were calculated to be 385(10) K and 330(10) K. Using the Debye model the f-factors for the whole temperature range were calculated. In the thin absorber approximation the intensity of an absorption line I is proportional to the effective thickness t given by

$$t = nf\omega\sigma_o,$$

where n is the number of resonant nuclei per unit area, ω is the relative transition probability and σ_0 is the resonance absorption cross section. In the paramagnetic region $\omega = 1/2$ for all individual lines, whereas in the ferromagnetic region ω varies betweeen 1/4 and 1/12 for the different lines in the sixfold sets. Taking the most intense lines as representative for the intensity we put $\omega = 1/4$ in the ferromagnetic region. Within the thin absorber approximation, the calculated relative intensities as functions of

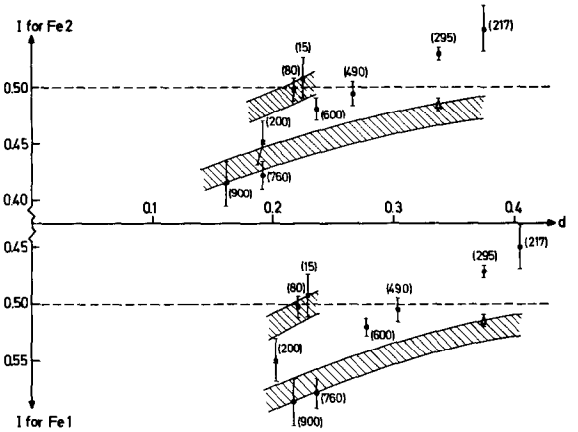

FIG. 4. Calculated relative intensities (shaded areas), in the absence of saturation effects, and experimental values for Fe(1) and Fe(2) as function of a reduced effective absorber thickness $d=f\cdot\omega$ (see Section 3.1). The numbers in parentheses are the temperatures of the measurements. ●, above T_c; ×, below T_c; △, from deconvoluted spectra.

absorber thickness on the assumption of equal occupation of Fe(1) and Fe(2) are shown in Fig. 4. The measured intensities, taken from Table II, are also shown in the figure and it is evident that for the smallest thicknesses good agreement is obtained only if Fe(1) in Table II is assigned to the Fe(1) position in the crystal. Our previous assignment (*14*), based on the room temperature measurement, is invalid due to the saturation effects that are clearly evident in Fig. 4. The result from the Fourier transformed spectrum is also included in Fig. 4 and it agrees well with the expectations based on the proposed assignment.

3.2. The Defect Structure of Nonstoichiometric Fe_2P and Related Compounds

Studies of the lattice parameter variation in nonstoichiometric Fe_2P (*6*, *10*) show that the unit cell dimensions decrease with decreasing iron/phosphorus atomic ratio. A similar contraction of the unit cells occurs in the isostructural phases Mn_2P and Ni_2P (*15*) and also in the closely related compound Co_2P (*23*). The contraction of the unit cells might be caused either by metal/phosphorus substitution or by the creation of metal vacancies. There are several reasons for rejecting the first alternative. In a structure, where some of the metal atoms are replaced by phosphorus atoms, very short P–P distances would inevitably occur. This situation is contrary to common crystal-chemical experience for structures of this type, where the tendency to avoid short P–P contacts is quite pronounced (*16*). Replacement of iron atoms by phosphorus atoms in Fe_2P would give P–P distances of 2.2–2.3 Å, while P–P distances in metal-rich transition metal phosphides normally exceed 3 Å. An analysis of the defect structure of Co_2P further supports the hypothesis of metal atom vacancies (*23*). A crystal structure refinement of a nonstoichiometric Co_2P crystal indicated a lower scattering parameter for one of the two nonequivalent cobalt positions. The assumption of P/Co substitution as responsible for the lower X-ray scattering led to a calculated P/Co atomic ratio far outside the limits of the phase-analytical results, while the assumption of cobalt vacancies was in full agreement with experimental data. The defect structure of Fe_2P is not easily susceptible to analysis by X-ray diffraction methods, since the preparation of nonstoichiometric crystals suitable for X-ray work is a difficult experimental problem. We therefore tried to use Mössbauer spectroscopy for the defect structure analysis.

The composition of Sample B corresponded to the formula $Fe_{1.957}P$. Assuming that the

TABLE II

RESULTS OF THE MÖSSBAUER MEASUREMENTS ON SAMPLE A[a]

Temperature (K)	Fe(1)				Fe(2)				
	B_{hf}	δ	Δ	I	B_{hf}	δ	Δ	I	Γ
900	—	−0.21(1)	0.13(1)	59(2)	—	0.17(1)	0.32(1)	41(2)	0.28(1)
760	—	−0.11(1)	0.13(1)	58(2)	—	0.30(1)	0.34(1)	42(2)	0.28(1)
600	—	−0.02(1)	0.11(1)	52(1)	—	0.40(1)	0.39(1)	48(1)	0.26(1)
490	—	0.06(1)	0.10(1)	51(1)	—	0.49(1)	0.40(1)	49(1)	0.27(1)
295	—	0.19(1)	0.10(1)	47(1)	—	0.61(1)	0.43(1)	53(1)	0.28(1)
220	—	0.26(1)	0.11(1)	47(3)	—	0.64(1)	0.43(1)	53(3)	0.35(1)
217	—	0.26(1)	0.09(1)	45(1)	—	0.64(1)	0.43(1)	55(1)	0.33(1)
215	—	0.24(1)	0.07(5)	41(5)	—	0.65(1)	0.43(2)	59(5)	0.35(1)
214	—	0.25(1)	0.10(2)	10(2)	—	0.65(1)	0.43(2)	12(2)	0.31(1)
	6.2(1)	0.34(1)	0.14(2)	44(2)	10.1(1)	0.61(1)	0.20(1)	34(2)	
200	7.7(1)	0.35(1)	0.14(2)	55(2)	12.4(1)	0.61(1)	0.22(1)	45(2)	0.30(1)
80	10.9(1)	0.41(1)	0.10(1)	50(1)	17.2(1)	0.66(1)	0.21(1)	50(1)	0.28(1)
15	11.4(1)	0.41(1)	0.10(1)	49(2)	18.0(1)	0.68(1)	0.19(1)	51(2)	0.33(1)

[a] B_{hf} is the magnetic hyperfine field in Tesla, δ the isomer shift in mm/s relative to iron metal at 295 K, Δ the electric quadrupole splitting in mm/s (defined as in Fig. 9), Γ the FWHM in mm/s and I the relative intensity in percent.

recoil-free fractions are unchanged on passing from Samples A to B, the expected intensity ratio I(Fe(1)): I(Fe(2)) was calculated in the thin absorber approximation in the paramagnetic region for (a) all vacancies on the Fe(1) position, (b) vacancies equally distributed over the two metal positions, and (c) all vacancies on the Fe(2) position. The results as well as the experimental ratios are presented in Table III. It is evident from the earlier discussion (Section 3.1) that the high temperature experimental ratio should be least affected by the systematic errors involved. A comparison of this ratio with the corresponding values for the three different models shows that model (c) gives the best agreement.

One would assume, in view of the thermal vibration parameters, that the Fe(1) atoms are more tightly bound in the structure, and the energy required for vacancy formation would accordingly be larger for Fe(1) than for Fe(2). It is interesting to observe that an analogous situation seems to prevail in Co_2P. The crystal structures of Co_2P and Fe_2P are different, but Co(1) and Co(2) are close counterparts to Fe(1) and Fe(2), respectively, both as regards the atomic environments and the thermal vibrations. In nonstoichiometric Co_2P, the vacancies are also most probably distributed on the Co(2) positions (*23*).

In order to provide material for further discussion, we undertook a structure refinement of a nonstoichiometric Mn_2P crystal with an estimated composition of $Mn_{1.9}P$. The results are presented in Table IV. For comparison, the results obtained previously for a stoichiometric Mn_2P crystal (*15*) are

TABLE III[a]

Temperature (K)	I(Fe(1))/I(Fe(2))			
	Model (a)	Model (b)	Model (c)	Experimental values
200	1.02(3)	1.07(4)	1.11(4)	0.89(11)
300	1.06(3)	1.10(4)	1.15(5)	1.00(2)
490	1.09(4)	1.14(5)	1.19(5)	1.32(6)
760	1.18(5)	1.24(5)	1.30(6)	1.44(7)

[a] Expected intensity ratios for Sample B at different temperatures, in the absence of saturation effects, calculated for (a) all vacancies on the Fe(1) positions; (b) vacancies equally distributed over both iron positions; (c) all vacancies on the Fe(2) positions.

TABLE IV

CRYSTALLOGRAPHIC DATA FOR Mn_2P AND $Mn_{1.9}P$

Atom	Position[a]	x		B(Å^2)		Degree of occupation	
		Mn_2P[b]	$Mn_{1.9}P$	Mn_2P[b]	$Mn_{1.9}P$	Mn_2P[b]	$Mn_{1.9}P$
Mn(1)	3 *f*	0.2546(4)	0.2532(6)	0.23	0.22(4)	1	0.88(3)
Mn(2)	3 *g*	0.5943(4)	0.5927(6)	0.43	0.48(5)	1	1
P(1)	2 *c*	$\frac{1}{3}$	$\frac{1}{3}$	0.40	0.33(8)	1	1
P(2)	1 *b*	0	0	0.40	0.58(14)	1	1

[a] Space group $P\bar{6}2m$.
[b] From (*15*).

included in the table. The scattering parameter value of 0.88(3) obtained for Mn(1) strongly indicates a vacancy concentration of about 10% on this position, which is entirely compatible with the estimated composition of $Mn_{1.9}P$ for the crystal concerned.

It is further evident from Table IV that the thermal vibration parameters change insignificantly on passing from the stoichiometric to the nonstoichiometric crystal. This supports indirectly the assumption we made for Fe_2P in interpreting the Mössbauer spectrum of Sample B.

The difference in vacancy distribution between Mn_2P on the one hand and Fe_2P and Co_2P on the other still remains to be accounted for. We propose a tentative qualitative explanation in terms of free energy differences as follows.

The thermal vibrations for the Me(2) atoms (Me = Mn, Fe, Co) are larger than those for the Me(1) atoms, which means that a larger entropy of vibrations is associated with the Me(2) atoms. We assume that for all three types of crystal the creation of vacancies at the Me(1) positions increases the internal energy more than a corresponding number of vacancies at the Me(2) positions. The free-energy contribution due to the entropy of mixing is the same, irrespective of the type of vacancies.

The difference in free energy between a crystal with only Me(1) type vacancies and a crystal with only Me(2) type vacancies will contain one positive term ΔU due to the difference in internal energies and one negative term $-T\Delta S$ due to the difference in vibrational entropy between the Me(2) and Me(1) atoms. As long as the ΔU term dominates, the crystal with Me(2) type vacancies will be the stable one. However, the $T\Delta S$ term increases with increasing temperature. Eventually, this contribution to the free energy might outweigh the ΔU contribution, and the crystal with Me(1) vacancies becomes the more stable one.

In our interpretation, Mn_2P which has the largest difference in thermal vibration parameters, conforms to the latter situation, while for Fe_2P and Co_2P the vibration entropy contribution is not large enough to balance the internal energy term at those temperatures, where an appreciable number of vacancies begin to be formed.

3.3. The Magnetic Structure of Fe_2P

As is evident from Fig. 5 and Table II there is a rather large difference in magnetic hyperfine field for the two iron atoms in the structure. If we assume that the same relation between magnetic moment and hyperfine field holds for both Fe(1) and Fe(2) we can derive values for the individual moments. Using the magnetic hyperfine field values obtained at low temperatures in the present study, and the recent magnetic moment value of 1.46(4) μ_B per iron atom (*24*) we obtain 1.14(4) μ_B and 1.74(4) μ_B for Fe(1) and Fe(2), respectively. From single crystal magnetization measurements it is known that the moments are directed along the *c*-axis (*24*).

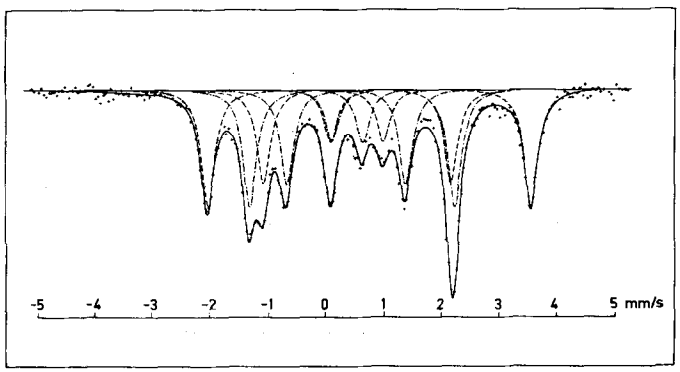

FIG. 5. Mössbauer spectrum of Fe_2P (Sample A) recorded at 80 K. Fe(2), ----; Fe(1), -·-·-.

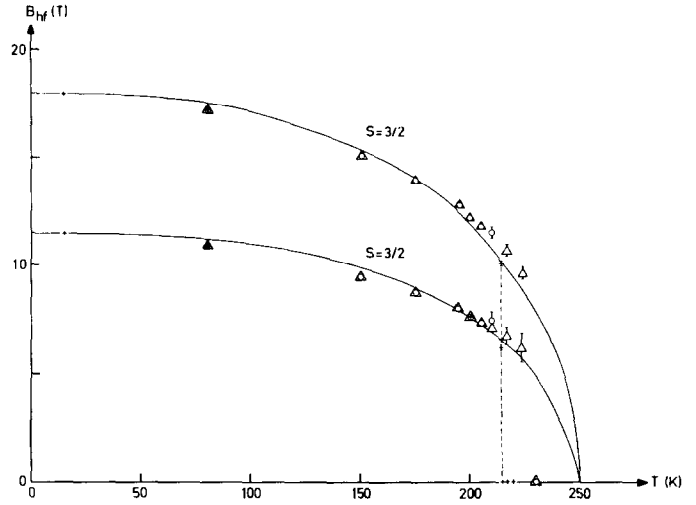

FIG. 6. Magnetic hyperfine fields as function of temperature. Sample A, +; Sample C, ○; Sample D, △.

Goodenough (*25*) has recently discussed the magnetic properties of transition metal pnictides M_2X in terms of the itinerant electron model assuming that only the 3*d*-bands have a finite density of states at the Fermi level, whereas the 4*s* band is empty. The magnetic properties therefore reflect only the number of 3*d* electrons per transition metal atom. In Fe_2P it is suggested that this number is $(6.5-\delta)$ and $(6.5+\delta)$ for Fe(1) and Fe(2), respectively. The corresponding magnetic moments have the spin-only values $(1.5-\delta)\ \mu_B$ and $(1.5+\delta)\ \mu_B$. Using the magnetic moments obtained above we can calculate δ to be 0.32(4) and the number of 3*d* electrons should be 6.18(4) for Fe(1) and 6.82(4) for Fe(2).

Using $\Delta R/R = -8.7\cdot10^{-4}$ (*26*) and the atomic Hartree–Fock electron densities calculated by Blomquist et al (*27*) for $3d^{6.18}4s^04p^0$ and $3d^{6.82}4s^04p^0$ and a relativistic correction [*28*], a difference in isomer shift of 0.27(4) mm/s is predicted between Fe(1) and Fe(2), the latter having the largest isomer shift with

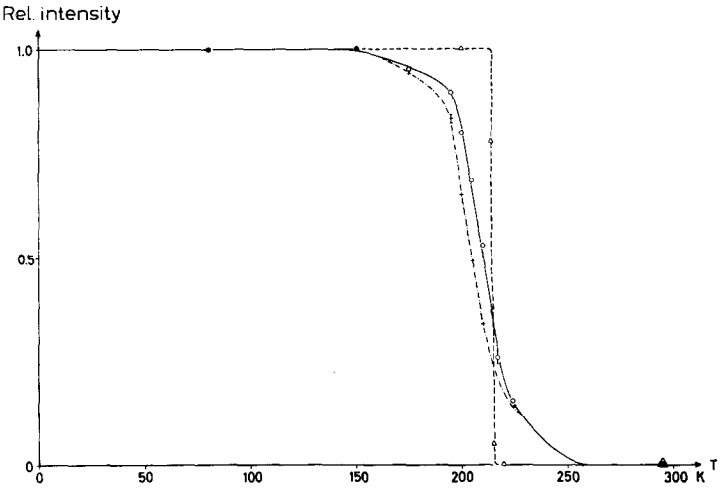

FIG. 7. Relative intensity of the ferromagnetic phase as a function of temperature. Sample C, +—·—·—; Sample D, ○———; Sample A, △– – – –.

respect to iron metal. This is in good agreement with the difference found experimentally (0.26(1) mm/s) and the relative order is also correctly described.

In order to obtain absolute agreement with the usual calibration curves for ^{57}Fe isomer shifts (calculated using ionic states) about one 4*s* electron has to be invoked. The difference can probably be as well explained by the fact that in Fe_2P, the *d*-electrons are only partly localized and hence are less effective in screening the 3s electrons from the nuclei.

3.4. The Magnetic Transition

As is evident from Fig. 6 the transition between the para- and ferromagnetic states does not display the usual Brillouin type behavior. The transition is well defined for Sample A occurring at 214.5(1.0) K, whereas for Samples C and D there is a rather large temperature region in which both a para- and a ferromagnetic structure is seen in the Mössbauer spectra. The relative intensity of the ferromagnetic part of the spectra is shown in Fig. 7.

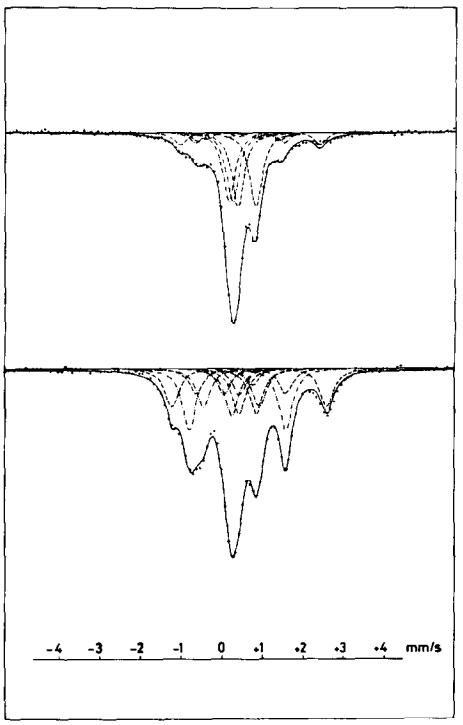

FIG. 8. Mössbauer spectra of Fe_2P (Sample D) at 217 K (top) and 205 K (bottom). Fe(2), ----; Fe(1),

The abrupt change of magnetization at the transition can be interpreted as due to a first-order transition. Several first-order transitions from antiferro- to paramagnetism have been reported involving 3*d* elements, e.g., $ZnCr_2O_4$ and $MgCr_2O_4$ (*29*), CrAs (*30*), and NiS (*31*). Among the lanthanides an example is afforded by europium metal (*32*), and it has recently been shown that also the transition in NpS is of this type (*33*). First-order transitions associated with the onset of ferromagnetism seem to be more scarce, MnAs (*35*) being one example. In those cases where the transition has been studied using the Mössbauer effect, a transition over an extended temperature range of the type found for Samples C and D (Fig. 8) is often reported.

It has been suggested that this broad transition region may be due to differences in temperature within the sample. In the present study this possibility can be ruled out since the boron nitride used in the absorbers is a good thermal conductor. Very recently (*36*) it has been shown that when mechanical strain is applied to the absorber, a broadening of the type found for Samples C and D is produced. We therefore suggest that since all hyperfine parameters are found to be closely the same for Samples A, C, and D, the origin of the transition region is due to microstrains, due for instance, to the presence of impurities or otherwise introduced during the thermal history of the samples. This view is further supported by the fact that for nonstoichiometric Fe_2P, Sample B, the transition region starts at ~160 K and proceeds to much lower temperatures.

In all the Fe_2P samples there is a change in electron density at the iron nuclei at the transition giving a discontinuous increase in isomer shift for Fe(1) of ~0.09 mm/s and a decrease of ~0.06 mm/s for Fe(2) (Fig. 9) on passing towards the ferromagnetic state.

From a point charge lattice sum using the formal valences of the metal atoms given by Goodenough (*25*) a calculation of the symmetry and direction of the efg tensor for

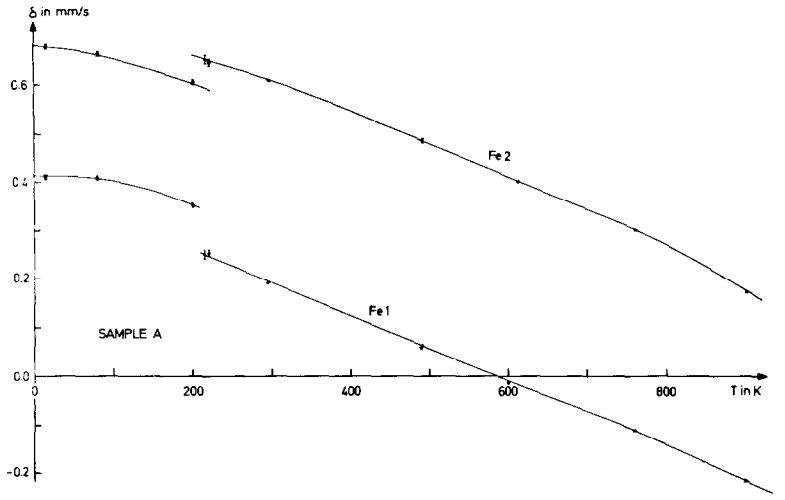

FIG. 9. The isomer shifts, relative to an iron metal absorber at 295 K, as function of temperature.

the two crystallographic iron positions was made. It was found, that the principal axis (V_{zz}) of the efg tensor was parallel to the c-axis for Fe(1), while for Fe(2) V_{zz} was perpendicular to the c-axis, and that the asymmetry parameter η of the efg tensor was 0.3 and 0.1, respectively. From a diagonalization of the full hyperfine hamiltonian with the above calculated values and the fact that the magnetic hyperfine fields are parallel to the c-axis (*24*) it seems that the change in Δ (Fig. 10) at the ferromagnetic transition is compatible with a constant electric quadrupole interaction (e^2qQ) for both lattice sites.

There have been several theoretical discusssions as to the mechanisms of first order magnetic transitions. All models assume that the free energy of the system under study contains additional terms besides the usual bilinear exchange hamiltonian. The first suggestion was that the biquadratic exchange term was of significance (*37*). This view was later critically examined by Harris (*38*) who showed that at least part of the deviations

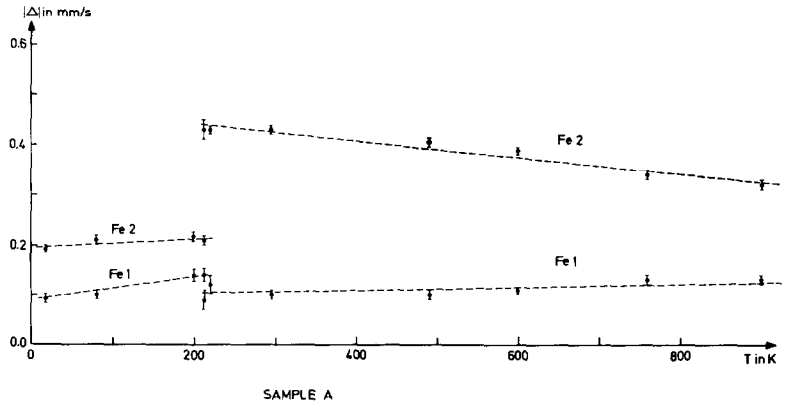

FIG. 10. Electric quadrupole splittings Δ as function of temperature. Above T_c, Δ is the doublet splitting, equal to $(e^2qQ)/2)\sqrt{(1+\eta^2/3)^{1/2}}$, and below T_c, the usual definition of Δ, when the electric quadrupole interaction is small compared to the magnetic, is used; i.e., $\Delta = (v_1 + v_6)/2 - (v_2 + v_5)/2$, where v_i is the velocity at the ith absorption line.

from Brillouin type behavior could be explained through more accurate calculations using the bilinear exchange hamiltonian. Lines and Jones (*39*) showed that the anomalies in the magnetization curves for MnO and MnS could be explained in terms of anisotropic magnetostrictive terms in the free energy. Blume (*40*) suggested that the first-order magnetic phase change could be interpreted in terms of the mixing of a low-lying excited state into the ground state through the action of a bilinear, isotropic exchange interaction. Later, Allen (*41*) examined the effects of quadrupole-lattice interaction terms in the hamiltonian.

As regards the magnetic transition in Fe_2P, the fact that a transition region is found for all samples (except for sample A where insufficient temperature stability is the most likely cause of the occurrence of two components at 214 K) indicates that the magnetoelastic effects are quite important in this compound. Preliminary X-ray diffraction studies (*42*) indicate that there is a change in lattice parameters of the order of 0.1 % at the transition.

In general, hysteresis effects are expected since in the ferromagnetic state the exchange energy is present and stabilizes this state to a higher temperature as compared to the passage from the paramagnetic to the ferromagnetic state. In the Mössbauer spectra no hysteresis was found. However, in the magnetization measurements on Sample A (*24*) a small hysteresis was observed and the ferromagnetic to paramagnetic transition occurred about 0.7° higher in temperature than the paramagnetic to ferromagnetic transition. The virtual absence of hysteresis in the Mössbauer measurements is probably due to the initially larger oscillations in temperature when the temperature is stabilized at a new value.

From Fig. 6 it is evident that the Curie temperature in the absence of the first order transition should occur at about 250 K in reasonable agreement with earlier magnetization measurements (*4*) using relatively strong magnetizing fields. It therefore seems that a strong external magnetic field will stabilize the ferromagnetic phase to higher temperatures.

It is interesting to note that the paramagnetic Curie temperature as deduced from the Curie–Weiss law is reported to be 464 K (*43*). The surprisingly large difference between ferro- and paramagnetic Curie temperatures indicates that the strength of the exchange interaction is strongly temperature dependent, being smaller at low temperatures.

4. Conclusions

From a detailed Mössbauer study an unambiguous assignment of the components in the spectra to the two nonequivalent iron atoms in Fe_2P has been made. The ordering of vacancies in nonstoichiometric Mn_2P and Fe_2P is found to be different, in Mn_2P the vacancies are predominantly found on Mn(1) positions, whereas in Fe_2P they are found mainly on Fe(2) positions. The magnetic hyperfine fields, extrapolated to 0 K are found to be $11.4(1)T$ and $18.0(1)T$ for Fe(1) and Fe(2), respectively. The corresponding magnetic moments are 1.14(4) μ_B and 1.78(4) μ_B, respectively and can be interpreted in terms of the itinerant electron model discussed recently by Goodenough (*25*). The magnetic transition is proposed to be of first order due to magnetoelastic effects. The isomer shifts show a discontinuous change at the Curie temperature 214.5 (1.0)K, whereas the electric quadrupole interaction seems to be fairly constant. The results indicate that the exchange interaction is strongly temperature dependent.

Acknowledgments

The authors thank Mr. B. Callmer for valuable assistance in the structure refinement of $Mn_{1.9}P$, and Dr. M. Richardson for correcting the English text of this paper. Financial support from the *Swedish Natural Science Research Council* is gratefully acknowledged.

References

1. S. CHIBA, *J. Phys. Soc. Jap.* **15**, 581 (1960).
2. A. J. P. MEYER AND M. C. CADEVILLE, *J. Phys. Soc. Jap.* Suppl. B-1 **17**, 223 (1962).
3. M.-C. CADEVILLE AND A. J. P. MEYER, *C. R. Acad. Sci. Paris* **252**, 1124 (1961).

4. M.-C. CADEVILLE, Thesis, University of Strasbourg (1965).
5. R. FRUCHART, A. ROGER, AND J. P. SENATEUR, *J. Appl. Phys.* **40**, 1250 (1969).
6. A. ROGER, Thesis, University of Paris (1970).
7. D. BELLAVANCE, J. MIKKELSEN, AND A. WOLD, *J. Solid State Chem.* **2**, 285 (1970).
8. A. CATALANO, R. J. ARNOTT, AND A. WOLD, *J. Solid State Chem.* **7**, 262 (1973).
9. A. GERARD, F. GRANDJEAN, AND M. WAUTELET *IV International Conference on Solid Compounds' of Transition Elements, Geneva* (1973).
10. B. CARLSSON, M. GÖLIN, AND S. RUNDQVIST, *J. Solid State Chem.* **8**, 57 (1973).
11. A. GÉRARD, *Bull. Soc. Belge Phys.* **1**, 43 (1966).
12. R. E. BAILEY AND J. F. DUNCAN, *Inorg. Chem.* **6**, 1444 (1967).
13. K. SATO, K. ADACHI, AND E. ANDO, *J. Phys. Soc. Jap.* **26**, 855 (1969).
14. R. WÄPPLING, L. HÄGGSTRÖM, S. RUNDQVIST, AND E. KARLSSON, *J. Solid State Chem.* **3**, 276 (1971).
15. S. RUNDQVIST, *Acta. Chem. Scand.* **16**, 992 (1962).
16. S. RUNDQVIST, *Ark. Kemi* **20**, 67 (1962).
17. D. AGRESTI, M. BENT, AND B. PERSSON, *Nucl. Instr. Methods* **72**, 235 (1969).
18. D. W. J. CRUICKSHANK, D. E. PHILLING, A. BUJOSA, F. M. LOVELL, AND M. R. TRUTER, "Computing Methods and the Phase Problem," p. 32. Pergamon, Oxford, 1961.
19. J.-O. LUNDGREN, Institute of Chemistry, Uppsala (1972) unpublished.
20. D. T. CROMER AND J. T. WABER, *Acta Cryst.* **18**, 104 (1965).
21. D. T. CROMER, *Acta Cryst.* **18**, 17 (1965).
22. M. C. D. URE AND P. A. FLINN, "Mössbauer Effect Methodology," Vol. 7, p. 245. Plenum Press, New York, 1971.
23. S. RUNDQVIST, *Acta Chem. Scand.* **14**, 1961 (1960).
24. L. LUNDGREN, O. BECKMAN, G. TARMOHAMMED, AND S. RUNDQVIST, *IV International Conference on Solid Compounds of Transition Elements, Geneva* (1973).
25. J. B. GOODENOUGH, *J. Solid State Chem.* **7**, 428 (1973).
26. P. H. BARRETT AND H. MICKLITZ, "Perspectives in Mössbauer Spectroscopy," p. 117. Plenum Press, New York–London, 1973.
27. J. BLOMQUIST, B. ROOS, AND M. SUNDBOM, *J. Chem. Phys.* **55**, 141 (1971).
28. D. A. SHIRLEY, *Rev. Mod. Phys* **36**, 339 (1964).
29. F. VARRET, A. GERARD, F. HARTMANN-BOUTRON, P. IMBERT, AND R. KLEINBERGER, *Proceedings of the Conference on the Application of the Mössbauer Effect (Tihany 1969)*, Akademiai Kiado, Budapest, p. 581 (1971).
30. H. BOLLER AND A. KALLEL, *Solid State Commun.* **9**, 1699 (1971).
31. J. M. D. COEY, H. ROUX-BUISSON, AND A. CHAMBEROD, to be published.
32. R. L. COHEN, S. HÜFNER, AND K. W. WEST, *Phys. Rev.* **184**, 263 (1969).
33. D. J. LAM, B. D. DUNLAP, A. R. HARWEY, M. H. MUELLER, A. T. ALDRED, I. NOWIK, AND G. H. LANDER, *International Conference on Magnetism, Moscow* (1973).
34. C. P. BEAN AND D. S. RODBELL, *Phys. Rev.* **126**, 104 (1962).
35. J. B. GOODENOUGH AND J. A. KAFALAS, *Phys. Rev.* **157**, 389 (1967).
36. G. R. DAVIDSON, M. EIBSCHÜTZ, AND H. J. GUGGENHEIM, *Phys. Rev.* **B 8**, 1864 (1973).
37. D. S. RODBELL, I. S. JAKOBS, J. OWEN, AND E. A. HARRIS, *Phys. Rev. Letters* **11**, 10 (1963).
38. E. A. HARRIS, *Phys. Rev. Letters* **13**, 158 (1964).
39. M. E. LINES AND E. D. JONES, *Phys. Rev.* **139**, 1313 (1965); and *Phys. Rev.* **141**, 525 (1966).
40. M. BLUME, *Phys. Rev.* **141**, 517 (1966).
41. S. J. ALLEN, *Phys. Rev.* **167**, 492 (1968).
42. L. LUNDGREN, Institute of Physics, Uppsala (private communication).
43. J. P. SENATEUR, A. ROUAULT, P. L'HERITIER, D. BOURSIER, A. KRUMBÜGEL-NYLUND, AND R. FRUCHART, *IV International Conference on Solid Compounds of Transition Elements, Geneva* (1973).